ACS SENSORS

pubs.acs.org/acssensors Article

Creation of a Nanobody-Based Fluorescent Immunosensor Mini Q-body for Rapid Signal-On Detection of Small Hapten Methotrexate

Akihito Inoue, Yuki Ohmuro-Matsuyama, Tetsuya Kitaguchi, and Hiroshi Ueda*

Cite This: https://dx.doi.org/10.1021/acssensors.0c01404 Read Online

ACCESS | Metrics & More | Article Recommendations | Supporting Information

ABSTRACT: "Quenchbody (Q-body)" is a quench-based fluorescent biosensor labeled with a fluorescent dye near the antigen-binding site of an antibody. Q-bodies can detect a range of target molecules quickly by simply mixing with a sample. However, the development of Q-bodies using V_{HH}-nanobodies derived from camelid heavy-chain antibodies has not been reported despite their favorable characteristics. Here, we report a "mini Q-body" that can detect the chemotherapy agent methotrexate (MTX) by using anti-MTX nanobody. Three kinds of constructs each encoding an N-terminal Cys-tag and anti-MTX VHH gene with a different length of linker $(GGGS)_n$ (n = 0, 2, and 4) between them were prepared followed by the expression in *Escherichia coli* and labeling with several dye maleimides. When the fluorescence intensities in the presence of varied MTX concentrations were measured, TAMRA-labeled nanobodies showed a higher response than ATTO520- or R6G-labeled ones. Especially, TAMRA C6-labeled mini Q-body with no linker showed the highest response of ~6-fold and a low detection limit of 0.56 nM. When each Trp residue in the mini Q-body was mutated to address the quenching mechanism, the major role of Trp34 at CDR1 in quenching was revealed. Furthermore, the mini Q-body could detect MTX in 50% human serum with a low detection limit of 1.72 nM, showing its applicability to therapeutic drug monitoring. This study is expected to become the basis of the construction of highly responsive mini Q-bodies for sensitive detection of many molecules from small haptens to larger proteins, which will lead to broader applications such as point-of-care tests.

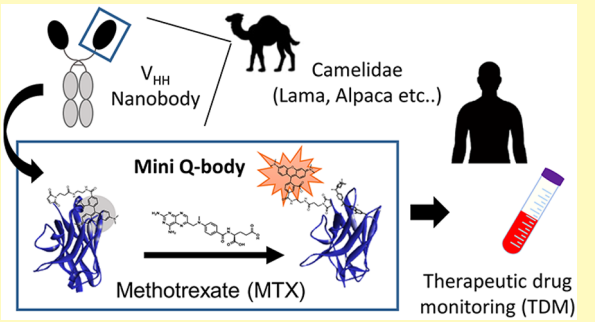

KEYWORDS: *immunosensor, quenchbody (Q-body), nanobody (V_{HH}), dihydrofolate reductase, point-of-care test, photoinduced electron transfer*

Immunoassays have become increasingly important in the field of biological and clinical research. Antibodies used for the immunoassay are capable of binding to antigens with high affinity and sensitivity, which are crucially important for the detection of a small amount of target antigens; for instance, highly sensitive detection of biomarkers in body fluids has been demanded for companion diagnostics.[1] Until now, various immunoassay methods have been developed; first developed in 1972 for example, enzyme-linked immunosorbent assays (ELISAs) are generally used in clinical diagnosis given their high sensitivity.[2] However, the multiple reaction steps and the requirement of technical expertise make the point-of-care test (POCT) difficult. Faster and handier methods such as immunochromatography are widely utilized, but their sensitivity is compromised with higher quantification demands.[3] To overcome such problems, our group sought to develop a fluorescent biosensor "Quenchbody (Q-body)", which is labeled with a fluorescent dye near the antigen-binding site of an antibody fragment such as a single-chain variable region (scFv) or Fab fragment.[4] Q-body can detect many target molecules from small haptens to large proteins based on the principle that the fluorescent dye quenched by the intrinsic tryptophan (Trp) residues shows antigen-dependent fluorescence recovery.[4,5] Since the conformational change of antibody fragments is induced by antigen binding, the internally quenched dye is displaced to the outside of the antibody fragment, leading to increased fluorescence. Compared to conventional ELISAs, Q-body-based assays not only are simple and rapid but also have a similar sensitivity to competitive ELISAs[a], without requiring time-consuming incubation and washing steps.[6−9]

Meanwhile, the novel antibody fragment, nanobody (also called V_{HH}), has become a powerful biological tool since it was found in 1993.[10] Nanobody is a single variable domain derived

Received: July 9, 2020
Accepted: October 23, 2020

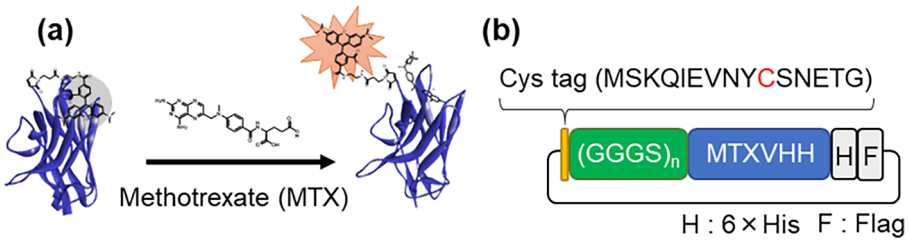

Figure 1. (a) Schematic image of mini Q-body. (b) Schematic structure of the coding region of pSQ-MTXVHHs.

from the heavy-chain-only antibody in Camelidae, and it can be characterized by its lower molecular weight and the smaller paratope than other antibody fragments such as scFv or Fab have, which makes nanobody capable of binding to concave and hidden epitopes[11] with similar affinity to conventional antibody.[12] Also, nanobody has an additional disulfide bond and several substitutions in the hydrophobic residue related with the V_H-V_L interaction, which results in the robustness to harsh conditions (i.e., high solvent concentration and high temperature)[13] and high production yields in various bacterial hosts.[14] If the nanobody can be employed to extend the Q-body approach, its outstanding property could favor the nanobody-based Q-body over the scFv- or Fab-based Q-body in the diagnostic application *in vitro*[15] or molecular imaging *in vivo*.[16] In this study, a nanobody that recognizes a small hapten methotrexate (MTX) was selected because it has a high affinity (5 ± 2 nM) to MTX and the structures with and without bound ligand were already solved,[17] which enabled the strategic design and analysis of resultant mini Q-bodies.

Also, MTX has been an important assay target due to its importance as a chemotherapeutic agent. Effects of MTX extend not only to cancer cells but also to normal cells and disrupt the activity of dihydrofolate reductase, which plays a critical role in DNA synthesis.[18] Hence, the blood concentration of MTX should be monitored to minimize the side effects, even when high doses of MTX are administrated for cancer chemotherapy.[19] This has attracted much attention for the development of an immunoassay method that will quantify MTX in human blood. Several human MTX ELISA kits have already been commercialized, and other immunoassay methods such as fluorescence polarization immunoassay (FPIA),[20] chemiluminescent microparticle immunoassay,[21] and enzyme multiplied immunoassay technique[22] were established to meet the practical demand for therapeutic drug monitoring (TDM). Although low limits of quantification (~50 nM) were achieved by these methods, the demand for further sensitivity and usability would remain.

Therefore, we aimed to construct a nanobody-based "mini Q-body" that can detect MTX at clinically sufficient levels (Figure 1a). As such, a Cys-tag containing a Cys residue for labeling a dye was introduced at the N-terminus of nanobody and the optimal structure of mini Q-body explored by varying the linker length and the fluorescent dye to achieve the desired response. Finally, detection of MTX was successful in up to 50% human serum using the mini Q-body at the normal concentration range for MTX TDM.

MATERIALS AND METHODS

Materials. *Escherichia coli* XL-10 Gold (Agilent, Santa Clara, CA, USA) and SHuffle T7 Express lysY (New England Biolabs Japan, Tokyo, Japan) were used for general cloning and protein expression, respectively. Plasmid pEX-K4J2-3QXV encoding $(GGGS)_4$ linker and anti-MTX nanobody[17] and all the oligonucleotides were synthesized at Eurofins Genomics (Tokyo, Japan). In-Fusion HD cloning kit and TALON metal affinity resin were obtained from Takara-Bio (Shiga, Japan). Restriction enzymes were purchased from New England Biolabs Japan. KOD-plus-neo DNA polymerase and Ligation High Ver. 2 kit were from Toyobo (Osaka, Japan). The PureYield plasmid miniprep and Wizard SV Gel and PCR clean-up kits were purchased from Promega (Madison, WI, USA). Anti-FLAG M2 magnetic beads, 3×DYKDDDDK peptide, and bovine serum albumin (BSA) were obtained from Sigma-Aldrich (St. Louis, MO, USA). ATTO520-C2-maleimide (mal) was purchased from ATTO-TEC (Siegen, Germany). Rhodamine 6G (R6G)-C2-mal, TAMRA-C5-mal, TAMRA-C6-mal, 5-TAMRA-C6-mal, and 6-TAMRA-C6-mal were obtained from Setareh Biotech LLC (Eugene, OR, USA). MTX was obtained from Nacalai Tesque (Kyoto, Japan). Human pooled serum (Cat. 2931149, Lot. S2225) was purchased from MP biomedicals (Irvine, CA, USA). Other chemicals and reagents, unless otherwise indicated, were obtained from Sigma-Aldrich or Fujifilm-Wako. All the water used was purified with a Milli-Q water purification system (Millipore, Billerica, MA, USA).

Construction of Expression Vector. Three kinds of constructs encoding an N-terminal Cys-tag, $(GGGS)_n$ linker (n = 0, 2, and 4), and anti-MTX nanobody (MTXVHH) gene were constructed. Initially, two MTXVHH fragments, one obtained from the *Age*I- and *Xho*I-digested fragment of pEX-K4J2-3QXV and the other amplified from pEX-K4J2-3QXV as a template using primers Inf_AgeI_back and Inf_XhoI_for, were cloned into the *Age*I- and *Xho*I-digested vector of pSQ(KTM219)[23] using ligation high ver2 and Infusion HD cloning kit, respectively. In addition to the resultant two construct, pSQ-MTXVHH and pSQ-GS4-MTXVHH, the $GGGS_2$ part in pSQ-GS4-MTXVHH was deleted by KOD plus mutagenesis kit using pSQ(3QXV)_(-8)_back and pSQ(3QXV)_(-8)_for to construct pSQ-GS2-MTXVHH. The nucleotide sequences of primers used are summarized in Supporting Information Table S1.

Expression and Purification of the Nanobodies. SHuffle T7 Express lysY cells were transformed with pSQ-GS(n)-MTXVHH (n = 0, 2, and 4) and cultured at 30 °C overnight in Luria-Bertani broth containing 100 μg/mL ampicillin (LBA) and 1.5% agar. A single colony was picked and grown at 30 °C in 4 mL of LBA medium overnight, and 2 mL of this culture was used to inoculate 200 mL of LBA medium followed by culturing at 30 °C. After the OD_{600} reached 0.6−0.8, 0.4 mM isopropyl-β-thiogalactopyranoside was added and the cells were incubated for an additional 16−20 h at 16 °C to express three kinds of nanobodies.

The cultured bacteria were collected by centrifugation at 5000*g* for 10 min at 4 °C, and the pellet was resuspended and disrupted in the 9 mL equilibration buffer (50 mM phosphate, 0.3 M sodium chloride [NaCl], pH 7.0) using a cell disruptor One shot model (Constant Systems Ltd., UK), from which cytoplasmic fraction was recovered. To purify the nanobodies, the supernatant was incubated with 0.4 mL of TALON immobilized metal affinity chromatography resin on a vertical tube rotator for 1 h at 4 °C. Afterward, the resin was washed twice with 10 mL of equilibration buffer and applied to the TALON gravity column (Takara-Bio). After washing with wash buffer (50 mM phosphate, 0.3 M NaCl, 33 mM imidazole, pH 7.0) once, the nanobodies were eluted by adding 200 μL of elution buffer (50 mM phosphate, 0.3 M NaCl, 500 mM imidazole, pH 7.0) thrice. The eluent was transferred into the G-25 Microspin column (GE

https://dx.doi.org/10.1021/acssensors.0c01404
ACS Sens. XXXX, XXX, XXX−XXX

Healthcare, Amersham, UK) to change the buffer to PBS, and the aliquot was taken for sodium dodecyl sulfate polyacrylamide gel electrophoresis (SDS-PAGE) analysis to determine the protein concentration comparing with varied concentration of BSA standard using a CCD camera (LuminoGraph, Atto, Tokyo, Japan).

Enzyme-Linked Immunosorbent Assay (ELISA). To prepare MTX−bovine serum albumin conjugate (MTX-BSA), MTX was activated by EDC-HCl and sulfo-NHS, and BSA was mixed with the activated MTX for 2 h at 25 °C. After gel filtration using G-25 PD-10 (GE Healthcare), the ratio of BSA/MTX was calculated from the absorbance spectrum between 240 and 400 nm using a UV−VIS spectrophotometer (V-730, JASCO). BSA and MTX-BSA were immobilized in the wells of a transparent polystyrene microplate (Costar 3590, Corning-Costar Japan, Tokyo, Japan) at 4 °C overnight, blocked with 20% ImmunoBlock (DS Pharma Biomedical, Osaka, Japan) at 25 °C for 2 h, and washed thrice with 10 mM phosphate-buffered saline (PBS) supplemented with 0.05% Tween20 (PBST). Afterward, the nanobody fragments in 100 μL of PBST containing 5% ImmunoBlock were applied and incubated for 1 h at 25 °C followed by three washes with PBST. The bound nanobodies were probed with 100 μL of 1/2000 diluted horseradish peroxidase-conjugated anti-His antibody in PBST containing 5% ImmunoBlock for 30 min at 25 °C. After washing three times with PBST, 100 μL of substrate solution (200 μg/mL 3,3′,5,5′-tetramethylbenzidine and 0.3 μL/mL (v/v) hydrogen peroxide in 100 mM sodium acetate, pH 6.0) was applied to the well. After incubation for 2−3 min, the reaction was stopped with 50 μL per well of 1 M sulfuric acid, and the absorbance was determined at 450 nm with a reference at 655 nm using a microplate reader (SH-1000Lab, Corona Electric, Ibaraki, Japan).

Preparation of Q-bodies from Recombinant Nanobodies. The purified nanobodies were labeled with maleimide dye to prepare mini Q-bodies. To this end, the exposed thiol group in the Cys-tag attached to nanobody was reduced mildly in 5 mM trisphosphine (TCEP) for 20 min at 25 °C, and TCEP was quenched in 20 mM 4-azidobenzoic acid for 10 min on ice as described previously.[24] Afterward, the dye maleimide (TAMRA-C5-mal, TAMRA-C6-mal, ATTO520-C2-mal, or R6G-C2-mal, 10 mM each in dimethylsulfoxide) was added to the solution and labeled in the dark for 2 h at 25 °C. The molar ratio of protein to dye was set to 1:10.

For each fluorescent dye-labeled protein, anti-M2 FLAG magnetic beads were used to remove the unreacted dye. The beads (10 μL) were added to the reaction solution and incubated for 1 h at 25 °C. Using a magnetic bead washer KingFisher (Thermofisher Scientific), the beads were washed 12 times in 200 μL of PBS containing 0.1% Briji35 and twice in PBST and incubated in 100 μL of PBST containing 150 μg/mL 3×DYKDDDDK peptide for 30 min at 25 °C, where the purified dye-labeled proteins were eluted. After SDS-PAGE analysis, a fluorescent image was obtained using a transilluminator with excitation set at 500 nm (Gelmiére, Fujifilm-Wako) for ATTO520- and R6G-labeled protein and a CCD camera (LuminoGraph, Atto) with excitation at 525 nm for TAMRA-labeled protein. The concentration of fluorescent dye-labeled protein was determined as described in the determination of unlabeled nanobody concentration.

Fluorescence Measurement of Mini Q-bodies. Fluorescence intensity was measured using a fluorescence plate reader (Clariostar, BMG Labtech). Each mini Q-body was diluted at 1 nM in PBST, and 1 μM MTX was subsequently added to the solution. Also, to denature the protein and measure the degree of quenching, 7 M guanidium hydrochloride (GdmHCl) containing 100 mM of dithiothreitol (DTT) was used instead of PBST. Each solution (100 μL) was applied to the 96-well black microplate and measured for the fluorescence. The excitation and emission wavelengths were 535/585, 515/570, and 497/552 nm for TAMRA-, R6G-, and ATTO520-labeled Q-body, respectively. For TAMRA C6-labeled Q-body, after incubation with 0−1 μM MTX for 15 min at 25 °C, the fluorescence spectra were obtained at 25 °C using a fluorescence spectrophotometer (FP-8500, Jasco, Tokyo, Japan). Dose−response curves were drawn by fitting the intensities at the maximum emission wavelength using a curve fitting function of MATLAB (Mathworks, Natick, MA). The EC50 value was calculated from the curve fitting to a modified 4-parameter logistic (4PL) equation. In detail, after normalizing the signal by the mean of the blank signal (w/ antigen per w/o antigen), the data except the blank was used for fitting to the modified 4PL equation as below, where minimum asymptote was fixed as 1 and C was estimated as EC50, while B is the Hill's slope and D is the normalized maximum asymptote.

$$y = D + \frac{1 - D}{1 + \left(\frac{x}{C}\right)^{B}}$$

The modified 4PL equation was applied to the Four parameters logistic regression function in MATLAB,[25] and goodness-of-fit measures including the coefficient of determination R^2 was obtained. A 95% confidence interval value for coefficient C was used as the standard error of EC50.

The limit of detection (LOD) was obtained as the estimated antigen concentration equal to the mean blank value plus 3 standard deviations (SD). LOD was obtained by two methods: from the fitted 4PL curve using one plus 3 SD of the blank value (n = 3) normalized by the mean blank signal or from the fitted straight line at three or four lower concentration including blank using mean blank plus 3 SD of the blank value (n = 3). LOD was decided as the value obtained from the method with the better goodness of fitting.

To evaluate the possible use of mini Q-body for TDM, a dose−response curve was drawn as above except that PBST with 50% human pooled serum and 5 nM Q-body were employed using a fluorescence plate reader. For the spike-and-recovery experiment, the human serum was spiked with MTX at four concentrations. After the samples were diluted five times by PBST, 30 μL was mixed with 5-TAMRA C6-labeled Q-body (5 nM, 30 μL) in PBST. The concentration of MTX in human serum was calculated from a dose−response curve in PBST, which was made by plotting the fluorescence intensity of standard solutions at different concentrations (0, 0.001, 0.003, 0.01, 0.03, 0.1, 0.3, 1, and 3 μM).

Mutagenesis of Trp Residues. To explore the quenching mechanism of 5-TAMRA C6-labeled Q-body without linker, the codons for Trp34, Trp38, Trp109, and Trp121 in the nanobodies were each replaced by that for Phe, which is similar in structure but with no quenching effect.[26] Two fragments were amplified using two combinations of primers, one is amplified with either W34F/W38F/W109F/W121F_back and T7 terminator and the other is amplified with either W34F/W38F/W109F/W121F_for and T7 promoter, for each mutant using pSQ-MTXVHH as a template, and the fragments were fused via splicing by overlap extension PCR. Each gene was digested with *Age*I and *Bam*HI, and the purified fragments were cloned into pSQ-MTXVHH, which were also digested with *Age*I and *Bam*HI.

Kinetic Analysis Using Biolayer Interferometry. To confirm the EC50 of 5-TAMRA C6-labeled Q-body that was derived from its dissociation constant (K_d), the K_d of 5-TAMRA C6-labeled Q-body was measured on the Octet K2 (Pall FortéBio, Menlo Park, CA). The sensor was constructed by loading biotin-NH_2 on the streptavidin (SA) sensor followed by reaction in 0.1 M MES (pH 5.5) containing 1 mM MTX and 20 mM EDC, which leads to the conjugation of the carboxy group of MTX to the amino group derived from biotin-NH_2 or SA. After setting a baseline in Kinetics buffer (PBS supplemented with 0.1% BSA and 0.002% Tween20), the sensor was dipped into Kinetics buffer containing 50, 100, 200, and 400 nM MTX for 300 s and in Kinetics buffer without MTX for 900 s for the measurement of the association rate and dissociation rate, respectively. The K_d value was calculated by global fitting in Data Analysis 8.1 HD software (Pall FortéBio).

RESULTS AND DISCUSSION

Confirmation of the Expression Level and Antigen-Binding Activity for Nanobodies. Three expression vectors encoding MTX nanobody were constructed and appended

https://dx.doi.org/10.1021/acssensors.0c01404
ACS Sens. XXXX, XXX, XXX−XXX

with an N-terminal Cys-tag and $(GGGS)_n$ linker (n = 0, 2, and 4). In these vectors, His- and FLAG-tags were added to the C-terminus of the nanobody to enable tandem purification necessary for dye-labeling of Q-bodies (Figure 1b). The sequences were confirmed by nucleotide sequencing, and the pSQ-MTXVHHs were successfully constructed. The vector was used to express and purify MTX nanobodies, and the expression level was estimated from the purified protein weight per cultured medium volume by SDS-PAGE. For each lane, a thick protein band at around 18 kDa was observed, which agreed well with the theoretical molecular weights of 17.0, 17.7, and 18.3 kDa for each sample, suggesting that they were correctly expressed as designed. As shown in Figure 2a, all the

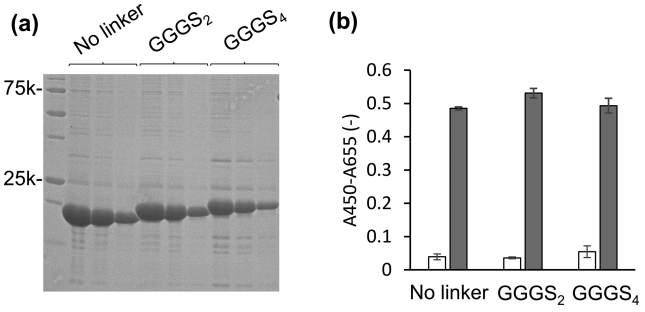

Figure 2. (a) CBB staining of SDS-PAGE for nanobodies. Three elutes for each sample are flow in three lanes. (b) Antigen-binding activity of nanobodies. Blank and filled bars represent ELISA signals with BSA and MTX-BSA (10 μg/mL each), respectively. Error bars represent ±1 standard deviation (SD) (n = 3).

MTX nanobodies were successfully expressed, and the shorter the linker length, the higher was the expression level. Moreover, the purified protein weights per cultured medium volume were calculated as 6.4, 5.2, and 3.7 mg/L for No linker, $GGGS_2$, and $GGGS_4$, respectively. These values were consistently higher than that of the scFv, which was expressed using pSQ-KTM219 under the same condition as MTX nanobodies (~1.0 mg/L) (data not shown). The nanobodies could meet the demand of large-amount protein when constructing Q-body due to the need for multiple purification steps.

In addition, the antigen-binding activity was evaluated by measuring the binding activity of the MTX nanobodies with immobilized antigen, MTX-BSA, using an ELISA. First, the UV spectrum of MTX-BSA showed that MTX was successfully conjugated with BSA (Figure S1). Indeed, MTX nanobodies showed antigen-binding activity in the ELISA using MTX-BSA (Figure 2b) with similar responses irrespective of linker length, suggesting that the MTX nanobodies retained their antigen-binding activity regardless of the additional Cys-tag and GGGS linker at the N-terminus.

Preparation of Q-bodies. The purified protein was labeled with maleimide dye at its Cys residue using maleimide−thiol reaction. After fluorescence labeling and re-purification by anti-FLAG beads, SDS-PAGE was performed to analyze the mobility and fluorescence of mini Q-bodies. At first, four types of maleimide dyes were used, including two TAMRA dyes with different linker structures. For each dye-labeled nanobody, one or two bands were observed in the CBB-stained gel, while one distinct band appeared in fluorescence gel images (Figure S2), suggesting that maleimide dyes were specifically labeled at the Cys residue of each nanobody. The additional band observed in the CBB stain of TAMRA-labeled nanobodies represents the dye-labeled nanobodies, which migrated faster than unlabeled nanobodies. The reason for higher mobility might be a more compact structure of dye-labeled denatured nanobodies, which indicates that TAMRA-labeled and unlabeled nanobodies coexist in the solution. Nevertheless, given the working mechanism of Q-body, small amount of the dye-labeled nanobodies should be enough to evaluate the single dye-labeled Q-body, whose response is barely influenced by its labeling yield.[4]

Q-body Assay. The Q-body activity of each labeled nanobodies was evaluated using a fluorescence plate reader. First, the fluorescent response upon denaturation by 7 M GdmHCl or the addition of 1 μM MTX was measured, which corresponds to the degree of quenching and antigen-dependent recovery, respectively. As shown in Figure 3, the

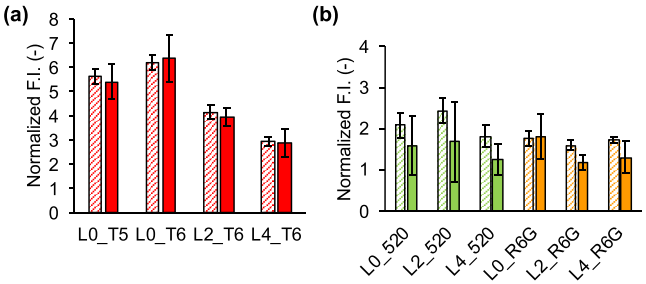

Figure 3. Quenching and antigen-dependent recovery of fluorescence-labeled nanobodies. (a) TAMRA derivatives and (b) others. T5, T6, 520, and R6G correspond to TAMRA C5, TAMRA C6, ATTO520, and Rhodamine 6G, respectively. L0, L2, and L4 correspond to MTX nanobody with no linker, GGGS2 linker, and GGGS4 linker, respectively. Hatched and filled bars represent the responses upon addition of denaturant (7 M GdmHCl, 100 mM DTT) and 1 μM MTX, respectively. The intensities were normalized by the mean fluorescence intensity of 1 nM Q-body in PBST. Error bars represent ±1 SD (n = 3).

fluorescent response of Q-bodies labeled with different dyes showed different degrees of quenching, and the TAMRA-labeled Q-body showed higher quenching than R6G- and ATTO520- labeled ones. Furthermore, the TAMRA-labeled Q-body without linker showed higher quenching; especially, TAMRA C6-labeled Q-body showed a 6.22-fold increase. Although the TAMRA C5 has a shorter linker between maleimide and dye than TAMRA C6, TAMRA C5-labeled Q-body showed lower quenching than TAMRA C6-labeled Q-body. In addition, R6G- and ATTO520-labeled Q-bodies showed less quenching than TAMRA-labeled Q-bodies, which indicates the crucial influence of the dye structure on quenching. Although the reason for the variable dye quenching cannot be precisely described, linker length and the different properties among fluorophores depending on the dye structure, including orientation, hydrophobicity, and molecular weight, are assumed to be the probable reasons; especially, the distance between the fluorophore and the Trp residues seems to be one of the most important factors. As previously described,[4,23] anti-osteocalcin (BGP) Q-body also showed different responses depending on its linker length and fluorophore, which indicates that the dye quenching could be influenced critically by the linker length and the dye structure.

https://dx.doi.org/10.1021/acssensors.0c01404
ACS Sens. XXXX, XXX, XXX−XXX

As expected, TAMRA C6-labeled Q-body also showed the highest antigen-dependent recovery, a 6.33-fold increase in fluorescence, while R6G- and ATTO520-labeled Q-body showed relatively low antigen responses, which might be due to greater quenching by free tryptophane.[27]

For further analysis of the TAMRA C6-labeled Q-body, the fluorescence spectrum was measured using a fluorescence spectrophotometer in the presence of 0−1 μM MTX. As shown in Figure 4, the maximum peak of fluorescence

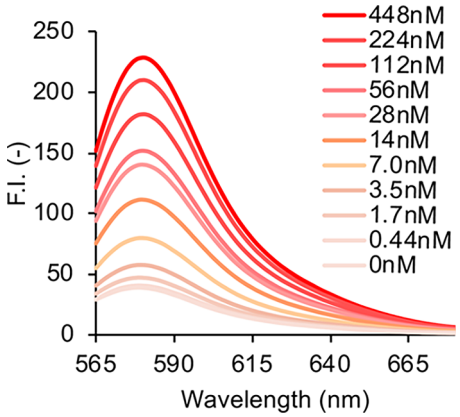

Figure 4. Fluorescence spectra of TAMRA C6-labeled Q-body without GGGS linker upon addition of indicated amounts of MTX.

appeared at around 580 nm, which corresponds with the spectrum of TAMRA dye, and the fluorescence intensity increased depending on the MTX concentration. Then, dose−response curves were drawn for TAMRA C6-labeled Q-body with different GGGS linkers by fitting the intensities at the maximum emission wavelength by curve fitting (Figure 5). The

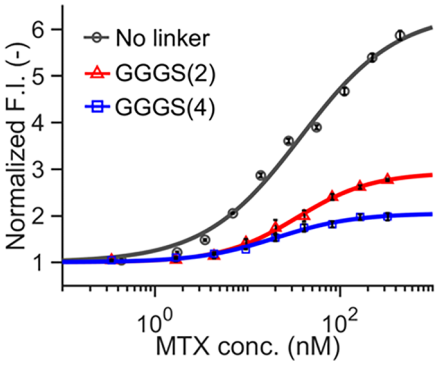

Figure 5. Dose−response curve of TAMRA C6-labeled Q-body with different-length linker at 0− 1 μM MTX. Error bars represent ±1 SD (n = 3).

result was in good agreement with the previous result for anti-BGP Q-body,[4] wherein the Q-body with a shorter linker showed a higher response. Also, EC50 values were calculated as 37.6 ± 11.0, 34.6 ± 13.8, and 20.4 ± 9.0 nM for the Q-body with No linker, $GGGS_2$, and $GGGS_4$, respectively, which were slightly higher but similar in value to the K_d obtained in the previous study (5 ± 2 nM).[17] Interestingly, TAMRA C6-labeled linker-less Q-body exhibited a lower LOD value (0.56 nM) compared with previous studies.[20−22] Since the goodness of linear fitting at the low concentration range of MTX (R^2 = 0.997) was better than that of 4PL fitting (R^2 = 0.988) (Figure S10), the value from the fitted straight line (0.56 nM) was adopted as the LOD. This value is less than 1/50 of the EC50 value, and it might not be generally observed in competitive ELISAs. However, the EC50 and limit of detection of anti-BGP Q-body were previously calculated as 116.8 ± 32.0 and 0.56 ± 0.20 nM, respectively,[28] suggesting lower error of Q-body assays due to the absence of multiple reaction/washing processes. Nevertheless, the low LOD of mini Q-body will indicate its potential utility to measure the lower concentration range of MTX required in clinical application.

Since TAMRA C6 contains two isomers, 5-TAMRA C6 and 6-TAMRA C6, the effect of tethering position was investigated (Figure S3a). When MTX nanobody without linker was labeled with these dyes, the 5-TAMRA C6-labeled Q-body showed a higher response than the 6-TAMRA C6-labeled Q-body (Figure S3b). Therefore, 5-TAMRA C6 with no GGGS linker was found as an optimal combination to construct mini-Q-body using MTX nanobody.

Analysis of the Quenching Mechanism. Previously, photoinduced electron transfer (PET) from the intrinsic Trp residues to fluorescent dye was revealed as a quenching mechanism of Q-body.[4] Therefore, the mutations were introduced into each Trp residue of the nanobody to confirm this. The wild type (WT) and W34F-, W38F-, W109F-, and W121F-mutated nanobodies without linker were constructed as before. After Q-bodies labeled with 5-TAMRA C6 were prepared, the fluorescent response upon denaturation or the addition of 1 μM MTX was measured for each Q-body, where 5-TAMRA C6-labeled W34F showed no fluorescence quenching or the response upon adding antigen. On the contrary, other mutants showed similar quenching to WT (Figure S4a), which suggests that Trp34 plays a major role in quenching compared with other Trp residues. The lower MTX-dependent fluorescence recovery of W109F and W121F seems to be caused by a decreased affinity due to each mutation (Figure S4b), while Trp38 at the core region (Figure S5) might play some role in quenching, as in the case of BGP Q-body.[4] The significant Trp34-induced quenching and its antigen-dependent recovery might be partly explained by the close proximity and the antigen-dependent change in distance between N-terminus and Trp34, calculated from the PDB structures (Figure S5); the Trp34 is the nearest to the N-terminus in the absence of antigen and moves significantly farther from this in the presence of antigen, which is not observed for other Trp residues. Additionally, the side chain of Trp34 interacts with MTX in the MTX-nanobody complex,[17] which implies direct inhibition of TAMRA−Trp34 interaction by the bound MTX.

As shown in Figure S6, while W34F mutant nanobody showed antigen-binding activity equivalent to that of WT, similar labeling efficiencies were confirmed for 5-TAMRA C6-labeled nanobodies. In addition, the peak wavelength of the fluorescence spectrum did not change compared with that of WT, which suggests that W34F mutation has negligible influence except for the reduced dye quenching.

It is worth noting that MTX shows little fluorescence that can enhance the fluorescence of the dyes used.[29] Also, MTX shows no absorbance at above 500 nm[30] and its electron-rich aromatic moiety that might cause PET is buried deeply in the MTX-nanobody complex,[17] which suggests the minimal possibility of MTX-induced quenching in the bound state. These considerations may contribute to understanding the possible quenching/de-quenching mechanism of this mini Q-

https://dx.doi.org/10.1021/acssensors.0c01404
ACS Sens. XXXX, XXX, XXX−XXX

Table 1. Binding Constants of the Proteins to Immobilized MTX

sample	k_{on} ($\times 10^4$ M^{-1} s^{-1})	k_{off} ($\times 10^{-4}$ M^{-1} s^{-1})	K_D ($\times 10^{-8}$ M)
MTX nanobody	1.28 ± 0.004	3.28 ± 0.02	2.57 ± 0.02
5-TAMRA C6-MTX nanobody	0.80 ± 0.09	2.00 ± 0.007	2.50 ± 0.03

body (Figure S7), which will be helpful to make the strategy of developing other mini Q-bodies for small haptens.

Similar Affinity of Mini Q-body to Nanobody. In previous studies, the fluorescence intensity of Q-body increased depending on the antigen concentration, which implies that the EC50 of Q-body would match the K_d of the fluorescent dye-labeled antibody. Therefore, to explore the K_d value of the fluorescent dye-labeled nanobody, kinetic analysis of the fluorescent dye-labeled nanobody was performed using biolayer interferometry. To this end, an MTX-loaded streptavidin sensor was prepared and the reaction time course between MTX and the unlabeled and 5-TAMRA C6-labeled MTX nanobody was monitored. A clear signal was obtained for both samples, and the 5-TAMRA C6-labeled MTX nanobody showed a higher response than unlabeled MTX nanobody (Figure S8), seemingly due to the increase in light absorption by the fluorescent dye that influences the light interference. Moreover, the K_d values obtained were 25.7 and 25.0 nM for unlabeled and 5-TAMRA C6-labeled MTX nanobody, respectively, using global fitting for four concentrations per sample (Table 1). The result suggested that the affinity of the MTX nanobody was minimally influenced by the fluorescent dye labeling and showed a similar value to the EC50. The single fluorescent dye (TAMRA) labeling had little influence on the nanobody affinity.

Performance of Mini Q-body in Human Serum. To explore the potential of mini Q-body in clinical applications, 5-TAMRA C6-labeled Q-body was used to measure MTX in the presence of human serum. When MTX is administered for chemotherapy, its concentration in human blood is maintained between 0.1 and 10 μM within 72 h after dose.[19] To evaluate the interference of human serum to the Q-body assay, the fluorescence intensity of 5-TAMRA C6-labeled Q-body was measured in the presence of 0−1.5 μM MTX in PBST and the 1:1 (v/v) mixture of human serum and PBST (50% human serum). As a result, the 5-TAMRA C6-labeled Q-body in 50% human serum showed a response that is in good agreement with that in PBST. Moreover, the Q-body exhibited low LOD (1.72 nM) (Figure S9); the goodness of fitting (R^2 = 0.983) and the response at 1.5 nM MTX, which is higher than the mean blank plus 3 SD of the blank value (n = 3) (Figure S10), could validate the LOD value, suggesting that the mini Q-body retains high sensitivity despite the interference by the human serum components such as serum albumins and hemoglobins.

Therefore, the analyses of non-spiked and MTX-spiked samples at the four concentrations (0.2, 0.5, 1, and 2 μM) in quadruplicate were performed at a serum concentration of 10% and the Q-body at a lower concentration (2.5 nM) to demonstrate that the MTX in a practical sample can be quantified using the mini Q-body. As shown in Table 2, the recoveries from the spiked sample were within a range of 109.4−136.4%, which indicates that the response of mini Q-body was slightly promoted by the matrix. Nevertheless, this result showed that MTX in human serum could be quantified simply and rapidly without any purification step, which suggests the applicability of mini Q-body to the MTX TDM.

Table 2. Spiked Concentration and the Recovery of MTX

	recovery (%)	
spiked conc. (nM)	mean	RSD
200	110.6	5.5
500	109.4	4.7
1000	136.4	10.7
2000	132.7	17.6

CONCLUSIONS

In the present study, mini Q-bodies were successfully developed to detect low-molecular-weight antigen MTX, which had been considered challenging due to its smaller paratope compared with conventional antibodies. In addition to choosing an appropriate nanobody with high affinity, by exploring the suitable linker length and dye structure that allowed higher response, the mini Q-body could successfully detect MTX at the low concentration range suitable for TDM. Since there had been no prior attempt to make a nanobody-based Q-body, the first "mini Q-body" was characterized from two perspectives: quenching mechanism and binding kinetics. For the former, the "mini Q-body" was confirmed to work based on the same principle as Q-bodies based on scFv or Fab, while the major role of Trp34 at the antigen-binding loop in quenching was revealed.

The selected mini Q-body exhibited a low LOD (1.72 nM) in 50% human serum. As far as we know, this LOD is as low as those of existing molecular probes including nanomaterial optical probes for MTX detection.[31] Also, the Q-body assay could achieve simpler and faster quantitative detection than LC/MS or competitive assays such as FPIA or localized surface plasmon resonance-based nanobiosensors.[32] Hopefully, the mini Q-body will further close the gap between academic validation and clinical acceptance of a TDM assay.[33]

In general, nanobodies show higher expression levels than scFvs, and they have higher stability than other antibody fragments. This is preferable not only for the Q-body construction but also for practical application where accurate quantification of the target is needed. This work will become the basis to construct such mini Q-bodies for sensitive detection of not only small molecules but also larger proteins. In the future, construction of highly responsive mini Q-bodies based on many other nanobodies is expected to be possible for a range of applications such as POCT.

ASSOCIATED CONTENT

Supporting Information

The Supporting Information is available free of charge at https://pubs.acs.org/doi/10.1021/acssensors.0c01404.

Table S1 for primer sequences, Figures S1−S3 for the exploration of optimal condition, Figures S4−S7 and Table S2 for the examination of the quenching mechanism, and Figures S8−S10 for affinity measurement and human serum interference for mini Q-body (PDF)

https://dx.doi.org/10.1021/acssensors.0c01404
ACS Sens. XXXX, XXX, XXX−XXX

AUTHOR INFORMATION

Corresponding Author

Hiroshi Ueda − *Laboratory for Chemistry and Life Science, Institute of Innovative Research, Tokyo Institute of Technology, Yokohama, Kanagawa 226-8503, Japan;* orcid.org/0000-0001-8849-4217; Email: ueda@res.titech.ac.jp

Authors

Akihito Inoue − *School of Life Science and Technology, Tokyo Institute of Technology, Yokohama, Kanagawa 226-8503, Japan*

Yuki Ohmuro-Matsuyama − *Laboratory for Chemistry and Life Science, Institute of Innovative Research, Tokyo Institute of Technology, Yokohama, Kanagawa 226-8503, Japan*

Tetsuya Kitaguchi − *Laboratory for Chemistry and Life Science, Institute of Innovative Research, Tokyo Institute of Technology, Yokohama, Kanagawa 226-8503, Japan;* orcid.org/0000-0001-6701-1933

Complete contact information is available at: https://pubs.acs.org/10.1021/acssensors.0c01404

Author Contributions

A.I. carried out the experiments and wrote the manuscript draft. H.U. conceived the study, designed the experiments, and edited the manuscript. Y.O.M. and T.K. supported performing experiments and editing manuscript. All authors have approved the final version of the manuscript.

Funding

This work was supported in part by JSPS KAKENHI grant number JP18H03851 (to H.U.) from the Japan Society for the Promotion of Science, Japan, and by JST-Mirai grant number JPMJMI18D9 (to H.U.) from Japan Science and Technology Agency, Japan.

Notes

The authors declare no competing financial interest.

ACKNOWLEDGMENTS

We are deeply indepted to Peter Kristensen and Bhagat Banwait for fostering the idea and performing initial trials of making V_H-based mini Q-bodies. We also thank the Biomaterials Analysis Division, Open Facility Center, Tokyo Institute of Technology for DNA sequence analysis, and support from Dynamic Alliance for Open Innovation Bridging Human, Environment and Materials from MEXT, Japan.

ADDITIONAL NOTE

[a]For detecting small molecules such as haptens with only one epitope (monovalent antigens), competitive ELISA employing the competition between enzyme-labeled and non-labeled antigens in a sample is usually used. For detecting proteins having multiple epitopes, sandwich ELISA can theoretically achieve a higher sensitivity, which might outcompete Q-body assay in terms of sensitivity.

REFERENCES

(1) Batrla, R.; Jordan, B. W. M. Personalized Health Care beyond Oncology: New Indications for Immunoassay-Based Companion Diagnostics. *Ann. N. Y. Acad. Sci.* **2015**, *1346*, 71−80.

(2) Engvall, E.; Perlmann, P. Enzyme-Linked Immunosorbent Assay, Elisa: III. Quantitation of Specific Antibodies by Enzyme-Labeled Anti-Immunoglobulin in Antigen-Coated Tubes Eva. *J. Immunol.* **1972**, *109*, 129−135.

(3) Posthuma-Trumpie, G. A.; Korf, J.; van Amerongen, A. Lateral Flow (Immuno)Assay: Its Strengths, Weaknesses, Opportunities and Threats. A Literature Survey. *Anal. Bioanal. Chem.* **2009**, *393*, 569−582.

(4) Abe, R.; Ohashi, H.; Iijima, I.; Ihara, M.; Takagi, H.; Hohsaka, T.; Ueda, H. "Quenchbodies": Quench-Based Antibody Probes That Show Antigen-Dependent Fluorescence. *J. Am. Chem. Soc.* **2011**, *133*, 17386−17394.

(5) Ohashi, H.; Matsumoto, T.; Jeong, H.-J.; Dong, J.; Abe, R.; Ueda, H. Insight into the Working Mechanism of Quenchbody: Transition of the Dye around Antibody Variable Region That Fluoresces upon Antigen Binding. *Bioconjugate Chem.* **2016**, *27*, 2248−2253.

(6) Abe, R.; Jeong, H.-J.; Arakawa, D.; Dong, J.; Ohashi, H.; Kaigome, R.; Saiki, F.; Yamane, K.; Takagi, H.; Ueda, H. Ultra Q-bodies: Quench-Based Antibody Probes That Utilize Dye-Dye Interactions with Enhanced Antigen-Dependent Fluorescence. *Sci. Rep.* **2015**, *4*, 4640.

(7) Yoshinari, T.; Ohashi, H.; Abe, R.; Kaigome, R.; Ohkawa, H.; Sugita-Konishi, Y. Development of a Rapid Method for the Quantitative Determination of Deoxynivalenol Using Quenchbody. *Anal. Chim. Acta* **2015**, *888*, 126−130.

(8) Zhao, S.; Dong, J.; Jeong, H.-J.; Okumura, K.; Ueda, H. Rapid Detection of the Neonicotinoid Insecticide Imidacloprid Using a Quenchbody Assay. *Anal. Bioanal. Chem.* **2018**, *410*, 4219−4226.

(9) Sasao, A.; Takaki, M.; Jeong, H.-J.; Yonemitsu, K.; Ohtsu, Y.; Tsutsumi, H.; Furukawa, S.; Morioka, H.; Ueda, H.; Nishitani, Y. Development of a Fluvoxamine Detection System Using a Quenchbody, a Novel Fluorescent Biosensor. *Drug Test. Anal.* **2019**, *11*, 601−609.

(10) Hamers-Casterman, C.; Atarhouch, T.; Muyldermans, S.; Robinson, G.; Hammers, C.; Songa, E. B.; Bendahman, N.; Hammers, R. Naturally Occurring Antibodies Devoid of Light Chains. *Nature* **1993**, *363*, 446−448.

(11) Muyldermans, S.; Cambillau, C.; Wyns, L. Recognition of Antigens by Single-Domain Antibody Fragments: The Superfluous Luxury of Paired Domains. *Trends Biochem. Sci.* **2001**, *26*, 230−235.

(12) Gonzalez-Sapienza, G.; Rossotti, M. A.; Tabares-da Rosa, S. Single-Domain Antibodies as Versatile Affinity Reagents for Analytical and Diagnostic Applications. *Front. Immunol.* **2017**, *8*, 1−12.

(13) van der Linden, R. H. J.; Frenken, L. G. J.; de Geus, B.; Harmsen, M. M.; Ruuls, R. C.; Stok, W.; de Ron, L.; Wilson, S.; Davis, P.; Verrips, C. T. Comparison of Physical Chemical Properties of Llama VHH Antibody Fragments and Mouse Monoclonal Antibodies. *Biochim. Biophys. Acta, Protein Struct. Mol. Enzymol.* **1999**, *1431*, 37−46.

(14) Liu, Y.; Huang, H. Expression of Single-Domain Antibody in Different Systems. *Appl. Microbiol. Biotechnol.* **2018**, *102*, 539−551.

(15) De Meyer, T.; Muyldermans, S.; Depicker, A. Nanobody-Based Products as Research and Diagnostic Tools. *Trends Biotechnol.* **2014**, *32*, 263−270.

(16) de Vos, J.; Devoogdt, N.; Lahoutte, T.; Muyldermans, S. Camelid Single-Domain Antibody-Fragment Engineering for (Pre)-Clinical *in Vivo* Molecular Imaging Applications: Adjusting the Bullet to Its Target. *Expert Opin. Biol. Ther.* **2013**, *13*, 1149−1160.

(17) Fanning, S. W.; Horn, J. R. An Anti-Hapten Camelid Antibody Reveals a Cryptic Binding Site with Significant Energetic Contributions from a Nonhypervariable Loop. *Protein Sci.* **2011**, *20*, 1196−1207.

(18) Goldman, I. D.; Matherly, L. H. The Cellular Pharmacology of Methotrexate. *Pharmacol. Ther.* **1985**, *28*, 77−102.

(19) Treon, S. P.; Chabner, B. A. Concepts in Use of High-Dose Methotrexate Therapy. *Clin. Chem.* **1996**, *42*, 1322−1329.

(20) den Boer, E.; Koch, B. C. P.; Huisman, R.; de Jonge, R. Using Fluorescence Polarization Immunoassay for Determination of Erythrocyte Methotrexate Polyglutamates, a Quick and Easy Test? *Ther. Drug Monit.* **2014**, *36*, 819−823.

(21) Bouquié, R.; Grégoire, M.; Hernando, H.; Azoulay, C.; Dailly, E.; Monteil-Ganière, C.; Pineau, A.; Deslandes, G.; Jolliet, P. Evaluation of a Methotrexate Chemiluminescent Microparticle Immunoassay. *Am. J. Clin. Pathol.* **2016**, *146*, 119−124.
(22) Shi, X.; Gao, H.; Li, Z.; Li, J.; Liu, Y.; Li, L.; Zhang, Q. Modified Enzyme Multiplied Immunoassay Technique of Methotrexate Assay to Improve Sensitivity and Reduce Cost. *BMC Pharmacol. Toxicol.* **2019**, *20*, 1−7.
(23) Jeong, H.-J.; Kawamura, T.; Dong, J.; Ueda, H. Q-Bodies from Recombinant Single-Chain Fv Fragment with Better Yield and Expanded Palette of Fluorophores. *ACS Sens.* **2016**, *1*, 88−94.
(24) Henkel, M.; Röckendorf, N.; Frey, A. Selective and Efficient Cysteine Conjugation by Maleimides in the Presence of Phosphine Reductants. *Bioconjugate Chem.* **2016**, *27*, 2260−2265.
(25) Cardillo, G. *Four parameters logistic regression - There and back again*; 2012 https://it.mathworks.com/matlabcentral/fileexchange/38122
(26) Marmé, N.; Knemeyer, J. P.; Sauer, M.; Wolfrum, J. Inter- and Intramolecular Fluorescence Quenching of Organic Dyes by Tryptophan. *Bioconjugate Chem.* **2003**, *14*, 1133−1139.
(27) Ogawa, M.; Kosaka, N.; Choyke, P. L.; Kobayashi, H. H-Type Dimer Formation of Fluorophores: A Mechanism for Activatable, in Vivo Optical Molecular Imaging. *ACS Chem. Biol.* **2009**, *4*, 535−546.
(28) Jeong, H.-J.; Matsumoto, K.; Itayama, S.; Kodama, K.; Abe, R.; Dong, J.; Shindo, M.; Ueda, H. Construction of Dye-Stapled Quenchbodies by Photochemical Crosslinking to Antibody Nucleotide-Binding Sites. *Chem. Commun.* **2017**, *53*, 10200−10203.
(29) Pascu, M. L.; Staicu, A.; Voicu, L.; Brezeanu, M.; Carstocea, B.; Pascu, R.; Gazdaru, D. Methotrexate as a Photosensitiser. *Anticancer Res.* **2004**, *24*, 2925−2930.
(30) Young, K. L.; Xu, C.; Xie, J.; Sun, S. Conjugating Methotrexate to Magnetite (Fe_3O_4) Nanoparticles via Trichloro-s-Triazine. *J. Mater. Chem.* **2009**, *19*, 6400−6406.
(31) Karami, F.; Ranjbar, S.; Ghasemi, Y.; Negahdaripour, M. Analytical Methodologies for Determination of Methotrexate and Its Metabolites in Pharmaceutical, Biological and Environmental Samples. *J. Pharm. Anal.* **2019**, *9*, 373−391.
(32) Yockell-Lelièvre, H.; Bukar, N.; Toulouse, J. L.; Pelletier, J. N.; Masson, J.-F. Naked-Eye Nanobiosensor for Therapeutic Drug Monitoring of Methotrexate. *Analyst* **2016**, *141*, 697−703.
(33) Masson, J.-F.; Pelletier, J. N. Will Nanobiosensors Change Therapeutic Drug Monitoring? The Case of Methotrexate. *Nanomedicine* **2015**, *10*, 521−524.

https://dx.doi.org/10.1021/acssensors.0c01404
ACS Sens. XXXX, XXX, XXX−XXX